EFFECTS OF PARTICLE CHARACTERISTICS ON THE SHEAR STRENGTH OF CALCAREOUS SAND

Pham Huu Ha Giang *(corresponding author)*
Ghent University,
Department of Civil Engineering
905 B-9052 Zwijnaarde, Belgium
E-mail: huuhagiang.pham@ugent.be
Can Tho University,
Department of Civil Engineering
3-2 Street, Can Tho, Viet Nam
E-mail: phhgiang@ctu.edu.vn

P. O. Van Impe
Department of Geotechnical Eng. at JDN - Jan De Nul Group
Tragel 60, 9308 Hofstade-Aalst, Belgium

W. F. Van Impe
Ghent University,
Department of Civil Engineering
905 B-9052 Zwijnaarde, Belgium

Patrick Menge
Dredging International
Scheldedijk 30, 2070 Zwijndrecht, Belgium

Veerle Cnudde
Ghent University,
Department of Geology and Soil Science
Krijgslaan 281, S8 9000, Gent, Belgium

Wim Haegeman
Ghent University,
Department of Civil Engineering
905 B-9052 Zwijnaarde, Belgium

Keywords
shear strength, sphericity, particle shape, calcareous sand

Abstract

The paper presents a 3D analysis (3DA) to evaluate the particle shape and size of silica and calcareous sands. The particles of calcareous sand are found to be less spherical than those of silica and crushed calcareous sands. Furthermore, the results indicate that the average sphericity (SPH) holds an inverse relationship to the particle size. However, in each sample the larger particles have higher SPHs than the smaller particles. In addition, the 3DA yields smaller particles than the sieve analysis (SA). Owing to a variety of particle shapes, causing particle interlocking, especially for calcareous sand, the particles cannot pass through the sieves by their shortest dimension. This paper discusses the effects of particle characteristics on the shear strength properties. Although the calcareous sand shows higher peak and residual shear strength properties, it tends to reach a lower shear strength at a small shear strain and a lower dilation than the silica sand. Moreover, the findings prove that the residual shear strength increases with the mean particle size. The sample with smaller particles shows less dilation under low vertical stress, while high vertical stress yields less compression. The relationship between the particle shape and shear strength properties is discussed based on the 3DA results.

1 INTRODUCTION

Particle characteristics (shape and size) are very important parameters affecting the shear strength properties. The determination of these shear strength properties requires expensive laboratory testing, so correlations between shear strength properties and particle characteristics can become more meaningful for both the design and construction of soil foundations. In particular, for calcareous sands, the collection of representative samples for the field conditions is much more difficult. Almost all measured soil parameters do not reflect the exact soil state prior to seismic loading. Under these conditions, a change in the grain characteristics might occur in calcareous sands. The skeletal particles of calcareous sands are varied and diverse in their size, shape and ability to resist mechanical and chemical effects. They are very angular [1–3] and exist at a higher void ratio than silica sands [4–7].

In previous studies on granular soils, it is observed that the relationship between sphericity (SPH) and particle size is not evident in previous studies. For silica sands, the larger particles are the most spherical [8, 9]. However, the results for different types of material and the database of previous studies show that no unique relationship exists between grain size and grain shape [4, 10, 11].

Recently, Dewen et al. [12] confirmed an increase in SPH with decreasing particle size for beach sands.

To measure and quantify particle shape, a two-dimensional (2D) microscopic method is commonly used, not only to directly evaluate the roundness of the particle, but also to estimate the form of the particle based on visual 2D plane imaging. In the 2D method, the thickness of the particle is estimated by the shadow projection of the particle. Compared to a three-dimensional (3D) method, the 2D method has some disadvantages. For sample selection, handling fine particles one by one is very time consuming, particles are handled randomly and particle spacing is often not sufficient to allow a clear shadow between adjacent particles. Therefore, the result of the 2D analysis is dependent on the arrangement of particles to capture 2D images. Although the 2D method can provide particle morphology, it can underestimate the true SPH of the particles [13]. Moreover, owing to the variation in particle shape, the use of roundness charts for silica sands based on 2D plane images cannot be used to determine the roundness for calcareous sands. Indeed, the 2D method is more applicable to grains where the longest and intermediate axes of particles can be easily presented parallel to the surface, whereas the shortest axis is perpendicular. In recent years, some techniques have been developed to identify particle morphology in 3D, such as automated serial sectioning tomography (a practical way to rebuild the 3D image from a succession of 2D ones), scanning transmission electron microscopy tomography using electron beams instead of X-ray, and X-ray computed tomography.

The influence of grain size distribution (GSD) on the shear strengths of soils shows that well-graded sand gives a higher shear strength than uniformly graded sand [14, 15]. The shear strength increases due to gradation broadening. This effect is examined by the void ratio decrease as the range of particle sizes increases [16]. Currently, there is still no consensus regarding the effect of morphology (shape and size) causing an increase or decrease in the shear strength properties of silica sands. Several studies reported that the particle size gave no significant difference in the shear strength [16, 17]. In contrast, other studies [18–20] revealed that the increase in particle size led to an increase in the shear strength. In addition, flaky and angular particles are found to increase the shear resistance [16, 21]. Kara [22] also showed that the peak friction angle increased with an increasing particle size, but there was no significant impact of the particle size on the residual friction angle at the critical state. Furthermore, Vangla et al. [23] found that the particle size had no influence on the peak friction angle, but affected the residual friction angles.

Compared to silica sands, calcareous sands are found to show greater shear strength properties [1, 3, 24–26] and a dilative behavior at low relative densities [2]. This behavior reflects the greater interlocking in calcareous sand due to the effect of particle shape. Indeed, the angular and less spherical particles do not move around each other easily, causing an increase in the dilation compared with smooth and rounded particles. The limited rotation and movement of the particles result in an increase in the inter-particle contact and, consequently, the shear strength [3, 27]. In addition, it is clear that the differences in mineral composition and gradation between silica and calcareous sands cause the difference in the shear strength properties. Previous studies also show the specific gravities of calcareous sands greater than 2.7 and larger than those of silica sands (approximately 2.65). Additionally, silica sands are generally a uniform grade, whereas the particles of calcareous sands are very angular and vary in size and shape, producing well-graded distribution curves. In conclusion, the current results of particle characteristics correlated to the shear strength properties are limited, especially for calcareous sands.

In this study, 3D particle measurements and analyses based on the data collected using X-ray micro-computed tomography (X-ray CT) are performed on three fractions of particles of a calcareous sand to determine the particle size and shape. The particle size and shape indices such as the Corey shape index (CSI), disc-rod index (DRI) and true SPH of each fraction are presented. For comparison, 3D particle tests are also performed on the same fractions of particles of the crushed calcareous sand and a silica sand. Finally, the shear behavior of the calcareous sand is investigated and correlated to the particle sphericity for calcareous sands.

2 MATERIALS & METHODOLOGY

2.1 Materials

The tests are initially performed on two types of sands. The calcareous sand, Sarb sand (S), used in this study is obtained from an artificial island in Abu Dhabi, while Mol sand (silica sand) is taken from Antwerpen, Belgium.

The purpose of this study is also to determine the effect of crushing on the particle shape. Therefore, the S sand is crushed under two loading conditions (dynamic and static loadings). Thus, the dynamic crushing method using a vibrating table in accordance with ASTM D4253 [28] is selected because it yields much more crushed particles. New particles produced by S sand under

Table 1. Physical properties of the studied materials.

Physical properties	Mol	SMol	VS	S	S2	S3	S4	S5	S6
Specific gravity, G_s	2.637	2.787	2.787	2.787	2.787	2.787	2.787	2.787	2.787
Mean grain size, D_{50} (mm)	0.167	0.167	0.425	0.73	0.205	0.408	0.565	0.815	1.135
Uniformity coefficient, C_u	1.44	1.44	5.429	3.46	-	-	-	-	-
Coefficient of curvature C_c	0.93	0.930	0.809	1.12	-	-	-	-	-
Maximum void ratio, e_{max}	0.93	1.340	0.956	1.33	1.376	1.435	1.556	1.752	1.835
Minimum void ratio, e_{min}	0.581	0.843	0.508	0.903	0.933	0.973	1.042	1.172	1.224
Maximum dry density, $\rho_{d(max)}$ (g/cm^3)	1.668	1.512	1.848	1.464	1.441	1.412	1.365	1.283	1.253
Minimum dry density, $\rho_{d(min)}$ (g/cm^3)	1.366	1.191	1.425	1.196	1.173	1.144	1.09	1.013	0.983

dynamic loading are called VS sand. Following this, S, VS and Mol sands are sieved to separate every fraction of particles and to remove particles larger than 4 mm. In addition, S sand particles are then used to match the grain size distribution (GSD) of the Mol sand, called SMol, to investigate the effect of the different material with the same C_u on the shear strength properties.

For the 3D scan, each sample is prepared by collecting the particles of the fraction obtained from the sieve. The following fractions of the three sands (Mol, S, VS) are selected for scanning: No. 90: 160-250 μm (Mol and S2), No. 35: 500-630 μm (S4 and VS4) and No. 18: 1-1.25 mm (S6 and VS6). The physical properties of the studied sands and fractions of S (S2, S3, S4, S5, S6) and VS (VS4, VS6) sands are summarized in Table 1 and the grain size distribution (GSD) curves are shown in Figure 1.

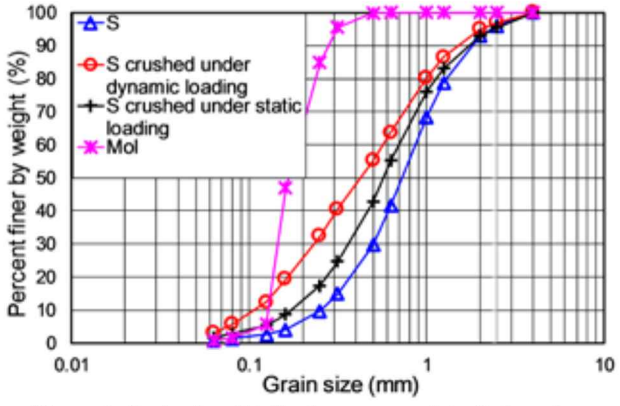

Figure 1. Grain size distribution curves of studied sands.

2.2 Methodology

3D particle evaluation and direct shear tests are performed in this study. The procedure of the 3D measurement and analysis consists of a scanner operation, tomographic reconstruction, 3D analysis (3DA) and visualization. The scanner operation is performed at the Center for X-Ray Tomography at Ghent University (UGCT). The whole system includes hardware for scanning and data acquisition and software tools for reconstructing radiographs and 3D visualization. These are briefly described below.

2.2.1 X-ray computed tomography

X-ray CT is a non-destructive technique to visualize the internal structure of objects and obtain 3D information regarding their shape. The X-ray CT device used in this study is a high-resolution X-ray CT (HRXCT) scanner developed by Masschaele et al. (2007) [29] at UGCT. Normally, an X-ray CT scanner includes an X-ray source and an X-ray detector connected to a computer. Unlike medical scanners, the source-detector is fixed, while the object, which is placed on a rotary stage (rotation angles from 0° to 360°) between the source and the detector, is rotated during scanning.

2.2.2 Octopus software

The software, Octopus (formerly known as Morpho+), is based on several algorithms and was developed in-house by Vlassenbroeck et al. (2007) [30] at UGCT. Octopus allows a determination of the porosity and the volume fraction of a component in the dataset [31]. Over the past few years, the program has been modified and extended to meet user demands and is now upgraded continuously. There are two separate packages to collect 3D information, the Octopus Analysis package and the Octopus Visualization package. The results of each step in the Octopus Analysis are shown in 2D, and Octopus Visualization is used to turn the analysis dataset 2D into a 3D view.

In order to evaluate the particle size, the maximum opening (MO) and minimum closing (MC) are calculated for each particle. MO is defined as the diameter

of the largest inscribed sphere in an object and MC is the diameter of the smallest circumscribed sphere in an object. The MO and MC of a particle are shown in Figure 2a. In the figure, MO is the lower limit for an object to pass through a virtual sieve mesh, while MC is used to determine the upper limit. For measuring the particle SPH, the equivalent diameter is defined as the diameter of a sphere with the number of voxels inside an object, and then the SPH of the object is calculated as the ratio of the MO to the equivalent diameter. In addition, an equivalent ellipsoid with the same moments of inertia as the object is used to calculate the disc-rod index and the shape index.

The analysis results are plotted on a diagram proposed by Illenberger [32] in which the Corey shape index (*CSI* defined as $S/(IL)^{1/2}$) is plotted against the disc-rod index ($DRI=(L-I)/(L-S)$) (L, I and S denote the longest, intermediate and shortest lengths of the particle, respectively). Illenberger's diagram delineates the areas for different types of shapes, including sphere, compact disc, compact blade, compact rod, disc, blade, rod, extreme disc, extreme blade, and extreme rod, as shown in Figure 3.

2.2.3 3D analysis

After acquiring the radiographs covering 360°, the tomographic reconstruction phase is processed to create 2D slices registered as 16-bit images by using the reconstruction software Octopus package. In the reconstruction phase, the obtained 2D projections are transformed into cross-sections through the sample using a filtered back algorithm. In the 3DA, the sample is expressed as a volume of voxels (3D pixels). The flowchart for the 3D particle analysis consists of loading the volume, filtering, thresholding, filling holes, labeling, distance map, object separation and rejoining, as demonstrated in Figure 2b. First, all the 2D slices obtained from the reconstruction volume are loaded into the computer memory. In this step, several parameters can be changed, such as the circular region of interest, the scale of data (16bit, 8bit) and the size calibration (voxel retrieved in μm). In the second step, i.e., filtering, the noise is removed using a bilateral filter (an extension of the Gaussian filter) to obtain clean images. For thresholding, the images are converted into binary images, with red and green representing the strong and weak thresholds, respectively. In this study, dual thresholding is applied to reduce the sensitivity to residual image noise. After thresholding, some voxels can be isolated if they are not connected to a voxel of the same binary value. Therefore, filling holes can help turning background voxels completely enclosed by foreground voxels into foreground voxels. In the fourth step, labeling is performed on the segmented images to assign a proper name to each particle based on foreground pixels in the binary image. For calculating the MO of a particle, the closest distance to the border of the particle is determined. This step is called the distance map. Additionally, after labeling, there is a remaining inter-connectivity between the particles due to the limited contrast or resolution of scanning, particle separation can be performed on the distance map of the

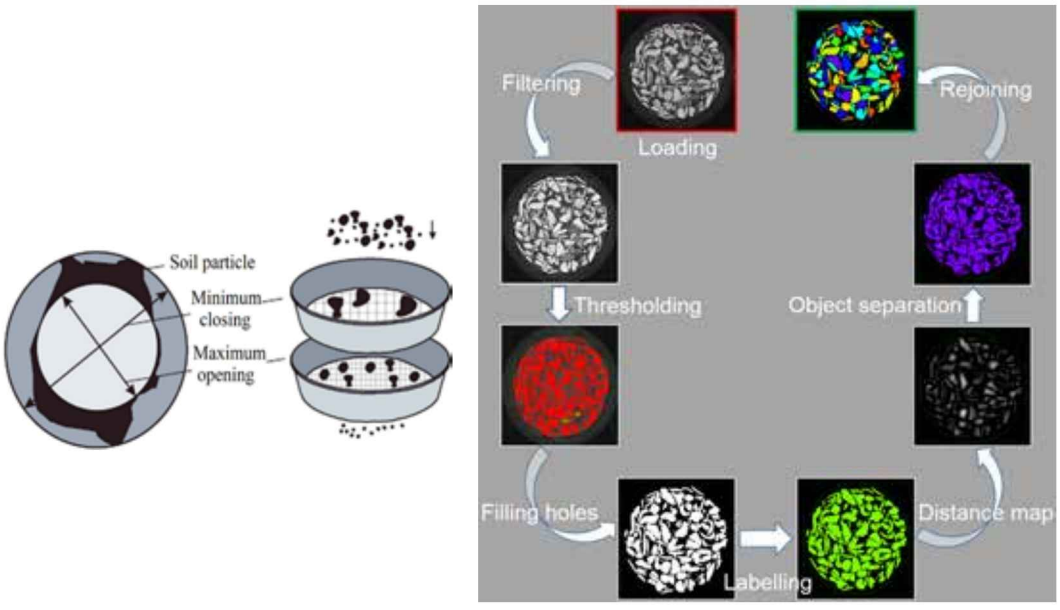

Figure 2. 3D analysis: (a) definition of MO and MC illustrated by Cnudde et al. [31], (b) Flow-chart of 3D analysis.

objects. In the final step, after separation, the software allows the manual rejoining or deleting of separated particles, or applying a smart rejoin operation. These steps are also described in previous studies [30, 33].

After rejoining, a script file of particles can be created that saves the particle properties, such as the number of particles; width, height, depth and volume of particles; equivalent ellipsoid; equivalent diameter; MC; MO; surface and SPH. The output data is extracted using MATLAB, and then transferred to Excel to perform the analysis efficiently.

2.2.4 3D visualization

The database of the 3D analysis is visualized by the package software Octopus 3D Viewer. The particles are rendered in arbitrary colors to present the contrast among individual particles with the different colors showing a variation of SPH (see Figure 6).

2.2.5 Direct shear tests

The second scope is to study the influence of particle morphology (shape and size) on the shear strength properties of calcareous sand and is conducted by direct shear tests. All the tested samples are molded into a metal shear box of 60 × 60 mm and 32.2 mm in height, consolidated at various normal stresses (50, 100, and 200 kPa), and sheared at a constant strain rate of 0.07815 mm/min. Due to the limit of horizontal displacement, all the tests are sheared up to 10% of the shear strain, which are considered as the residual shear strengths.

Two series of direct shear tests are performed. For series 1, the effects of particle shape and material composition of the silica sand (Mol) and the artificial calcareous sand (SMol) are studied. For series 2, the tests are performed on five fractions of S sand with different D_{50}. In the study, the Mohr-Coulomb failure criterion is used to obtain the peak and residual shear strength and internal friction angle of the sands. The dilation angle (ψ) is expressed by the ratio of incremental vertical displacement δ_y to the horizontal incremental displacement δ_x ($\tan\psi = \delta_y/\delta_x$). After shearing, a sieve analysis is also performed to determine possible crushing of the particles of the tested samples.

3 RESULTS AND DISCUSSION

3.1 3D particle shape

The distribution of the particle shape is plotted in Figure 3. In this figure, a significant difference in shape index for the same fraction of particles (160-250 μm) between silica sand (Mol) and calcareous sand (S2) is seen. The shape index in the Mol sand is found to be higher than that in S2. However, it is not easy to see the difference in the particle shape between the test samples due to the difference in the number of particles (N). Therefore, the percentage of particle shapes in each sample is demonstrated as in Figure 4. In Figure 4, the silica sample (Mol) contains more spheres and blades compared to rods and discs. In calcareous sand, the blades appear the most,

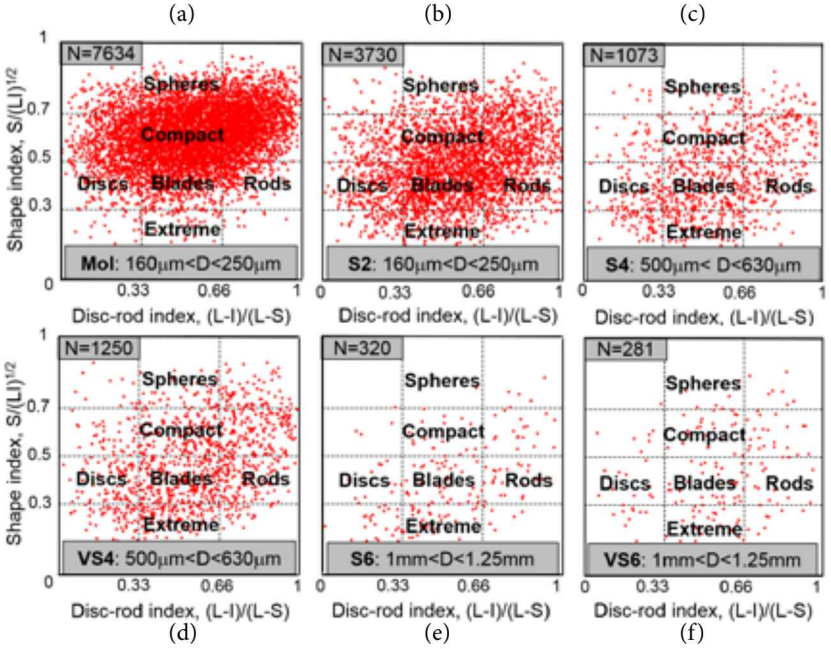

Figure 3. Form diagram of the tested samples (N is number of particles).

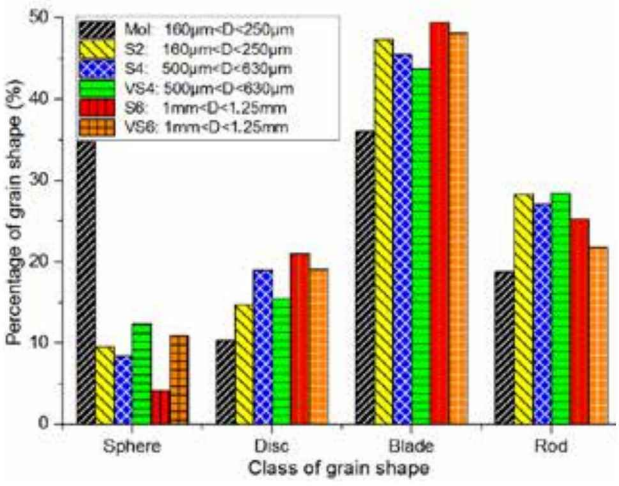

Figure 4. Percentage of grain shape.

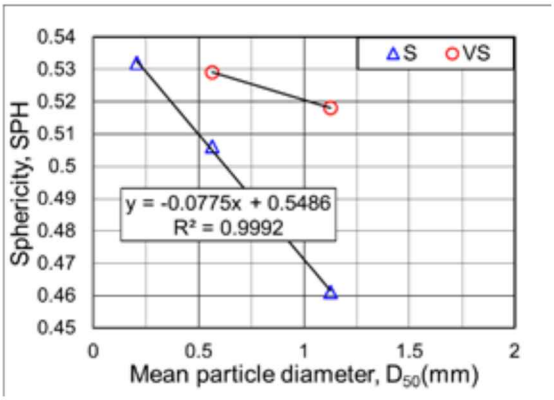

Figure 5. Relationship between sphericity and mean particle diameter.

followed by rods, discs and spheres. For S sand, the fraction of smaller particles tends to contain more spheres and rods and fewer discs than the fraction of larger particles. This is also found for the crushed samples (VS4 and VS6).

The main purpose of this 3D analysis is to determine the relationship between the grain shape and size for calcareous sand. Therefore, the average SPH of each sample and the mean grain size obtained by sieve analysis (SA) are given in Figure 5. It is observed from Figure 5 that the SPH increases with a decrease in the grain size. The best-fit curve is represented by a linear trend line, as shown in Eq. 1, with a very good coefficient of determination (R2 ≈1) for S sand.

$$SPH = -0.0775^{*} D_{50} + 0.5486 \qquad (1)$$

Further, Figure 5 shows that at the same particle sizes (500–630 μm and 1–1.25 mm) the crushed samples (VS4, VS6) give higher values of SPH than the S samples (S4, S6). In particular, both sands (S, VS) seem to have an equivalent SPH for small particles (D < 0.167 mm).

Figure 6 demonstrates the 3D rendered images of all the tested samples with the corresponding SPH values. The average SPH value in each sample is also mentioned in Figure 6.

In addition, the results of the 3DA are compared to those of the sieve analysis (SA). In Figure 7, it is clear that there is a significant difference in the grain size obtained with the two methods, in particular for calcareous sand. The 3DA gives smaller values of particle sizes than the SA. Figure 7 also shows a greater difference for the fraction of larger particles (smaller SPH). Apart from errors due to resolution that may occur in the 3D

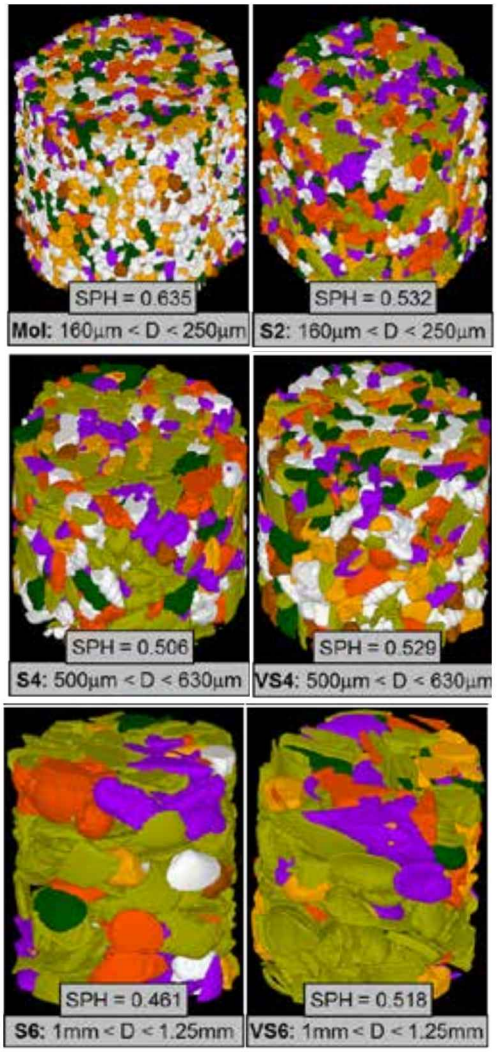

Figure 6. Simulated samples of silica and calcareous sands with 3D rendered by Octopus visualization.

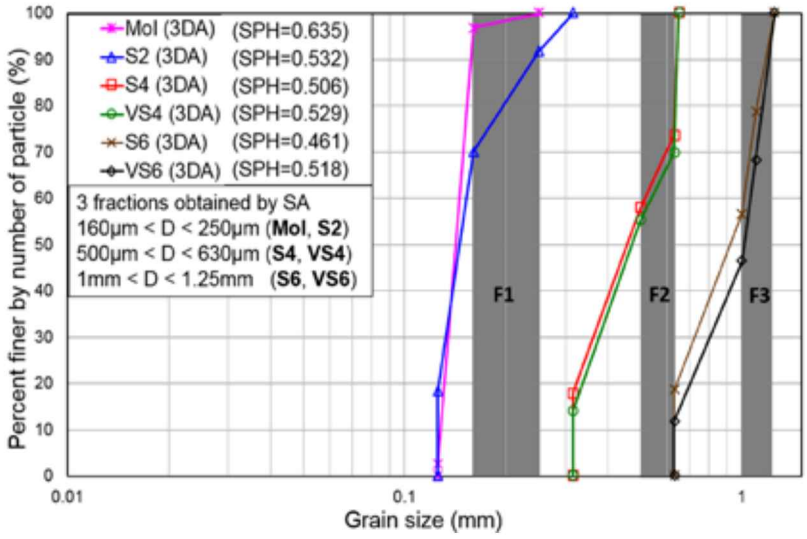

Figure 7. Comparison between 3DA and SA.

method, the difference between the results of SA and 3DA is mainly due to the effect of particle shape in this study. Namely, some particles can pass through the sieve by their intermediate or longest dimension, and particles are retained on the sieve owing to particle interlocking caused by various particle shapes. In this case, it can be concluded that the particle shape has an influence on the SA results. The difference in grain size distribution curves obtained by the 3DA between the VS and S samples are also presented in Figure 7. The difference becomes smaller in a smaller particle range. The results of the 3DA show that the VS samples (VS4, VS6) have larger particles than the S samples (S4, S6), but the VS samples have higher values of SPH. This means that after crushing the particle shape of calcareous sand tends to become more spherical, and the number of particles like blades or discs decreases (Figure 4).

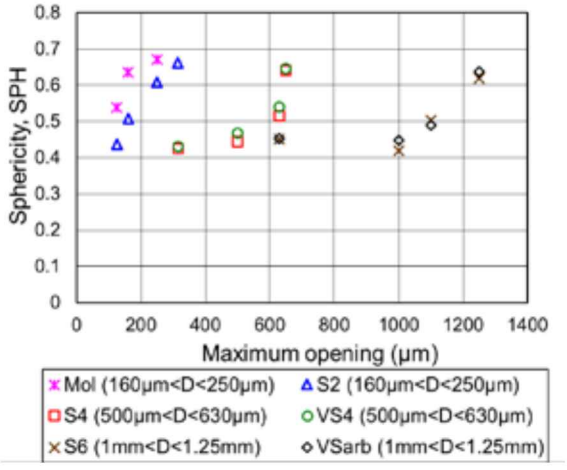

Figure 8. Relationship between sphericity and grain size (MO).

Figure 8 displays the relationship between SPH and MO for each sample. The results show that there is a similar tendency in each sample with MO increasing with an increasing SPH. It is noted that particles with greater SPHs pass through a sieve more easily. As a result, in each sample the smaller particles have lower SPHs than the larger particles.

It is known that the void ratio is dependent on the shape of the particles. In this study, the determination of the maximum and minimum void ratios is considered as an alternative method to see the effect of particle shape on density. The results conducted according to the Japanese Geotechnical Society standard JIS A 1224, 2009 [34] are shown in Table 1. It is clear that the void ratios of SMol are higher than that of Mol sand. This is a reasonable result and once again confirms the results of the 3DA as the void ratios (e_{max} and e_{min}) decrease with increasing SPH.

3.2 Effects of particle characteristics on shear strength properties

The results of the direct shear tests are plotted as shear stress versus shear strain, and as vertical displacement against shear strain (Figure 9). Table 2 summarizes all the results of the direct shear tests. The void ratio and relative density after the consolidation of each tested sample are mentioned in the table. Based on the results of the sieve analysis, there is no crushing after shearing in all the tested samples.

3.2.1 Comparison of calcareous and silica sands

The comparison of the test results of Mol and SMol sands for medium and dense samples (D_r = 40%, D_r =

Table 2. Direct shear test results.

Sample	Normal stress σ'_v (kPa)	Dry density ρ_d (g/cm3)	Void ratio e	Relative density, D_r (%)	Peak shear strength, τ_p (kPa)	Peak friction angle, ϕ_p (°)	Residual shear strength, τ_r (kPa)	Residual friction angle, ϕ_r (°)	Maximum dilation angle, ψ_{max} (°)
SMol	50	1.315	1.119	44.6	-	-	30	30.9	5.4
	100	1.323	1.106	47.0	-	-	63	32.1	6.3
	200	1.331	1.094	49.5	-	-	137	34.5	1.6
	50	1.445	0.928	82.8	40	38.6	38	36.9	11.2
	100	1.450	0.922	84.1	74	35.3	71	35.2	7.0
	200	1.463	0.904	87.6	167	39.9	157	38.1	2.3
Mol	50	1.486	0.774	44.7	-	-	28	28.4	9.5
	100	1.496	0.762	48.0	-	-	56	29.4	7.6
	200	1.510	0.747	52.5	-	-	116	30.1	4.8
	50	1.604	0.644	81.9	36	36.1	31	31.5	12.7
	100	1.606	0.642	82.4	67	34.0	62	31.7	11.6
	200	1.610	0.638	83.7	148	36.4	135	32.1	13.9
S2	50	1.274	1.187	42.7	-	-	27	28.8	6.7
	100	1.285	1.168	46.9	-	-	63	32.1	5
	200	1.287	1.164	47.8	-	-	142	35.5	-
S3	50	1.243	1.242	41.9	-	-	28	29.2	9.3
	100	1.250	1.229	44.7	-	-	70	35.1	6.7
	200	1.257	1.217	47.3	-	-	146	36.1	-
S4	50	1.196	1.330	44.0	-	-	31	31.7	13.3
	100	1.203	1.317	46.5	-	-	75	36.7	10.8
	200	1.208	1.307	48.5	-	-	157	38.1	-
S5	50	1.114	1.501	43.3	-	-	32	32.9	12.6
	100	1.122	1.485	46.1	-	-	77	37.7	7.1
	200	1.133	1.459	50.6	-	-	163	39.2	-
S6	50	1.086	1.565	44.1	-	-	38	36.9	14.7
	100	1.096	1.543	47.8	-	-	89	41.6	6.7
	200	1.107	1.517	52.1	-	-	181	42.2	-

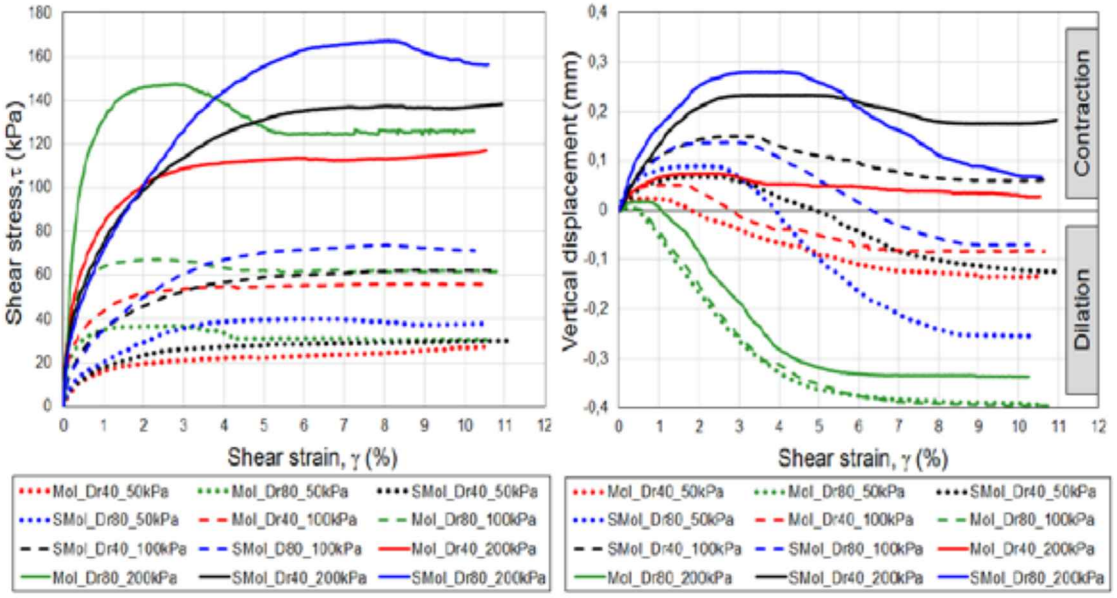

(a) Effect of difference in soil type, especially in particle shape (series 1)

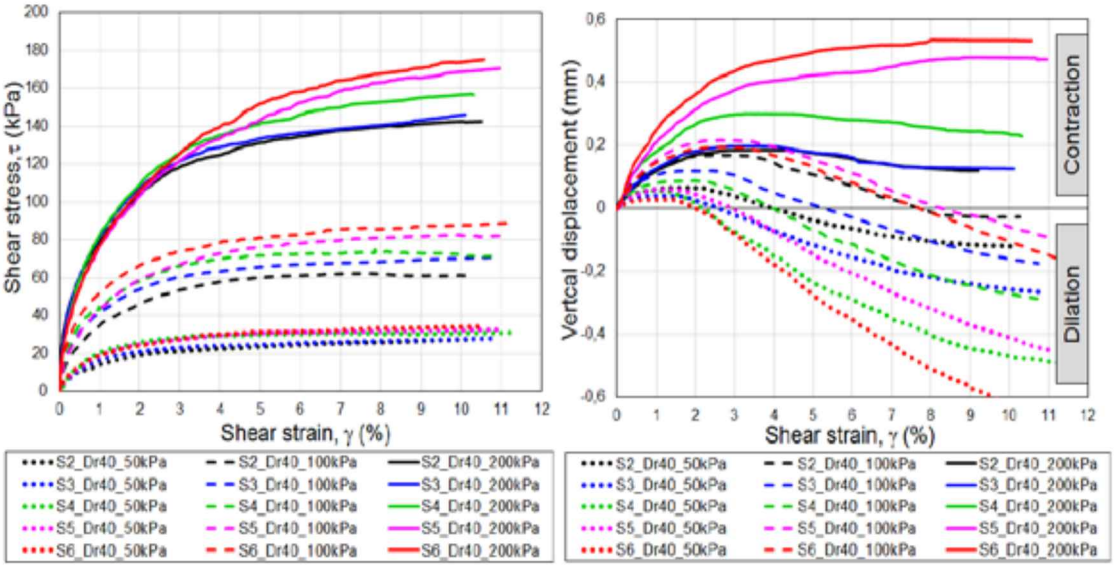

(b) Effect of mean grain size D_{50} (series 2)

Figure 9. Results of direct shear tests.

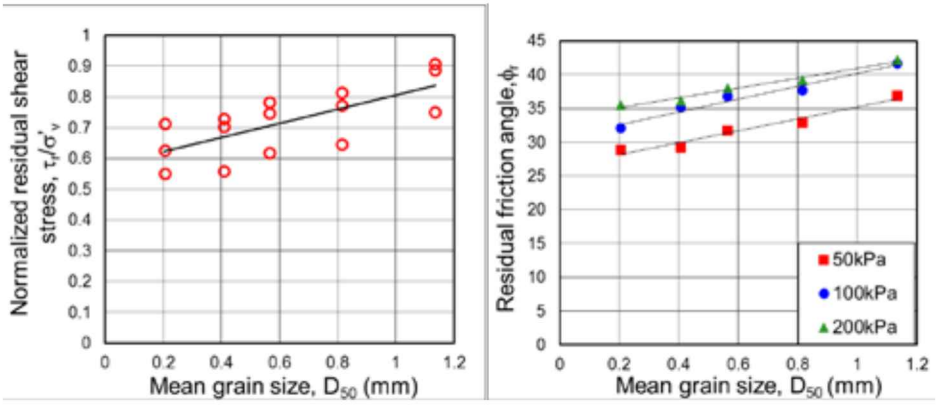

(a) Relationship between shear properties and D_{50}

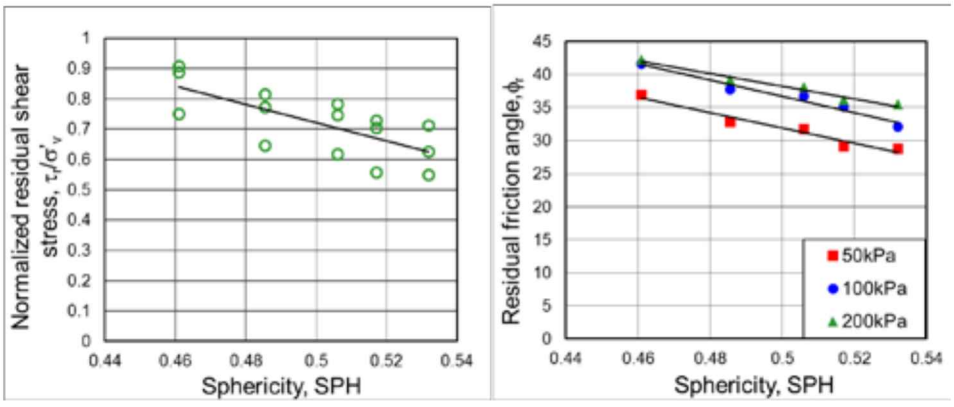

(b) Relationship between shear properties and sphericity (SPH)

Figure 10. Relationship between shear properties and particle characteristics (D_{50}, SPH) at various normal stress for medium dense samples.

80%) are shown in Figure 9a. As expected, an increase in the initial relative density and normal stress leads to an increase in the peak shear stress determined for both sands. In Table 2, the SMol sand has higher shear strengths and friction angles at the peak and residual states than Mol sand. Under constant normal stress, the difference in residual stresses between the samples at 40% and 80% of the initial relative density for Mol sand is less than that in SMol sand. These results indicate that the initial relative densities of the samples have an influence on the shear strength and friction angle at the residual state (γ = 10%), which is significant for calcareous sand. From the literature, the critical state is found to be independent of the initial relative density, suggesting that to reach a critical state in each test, the tests should be performed to a higher shear strain (e. g, γ = 15% or 20%).

Figure 9a further shows that dilation is observed in most of the tests at the end of shearing. The dense samples are found to have a higher dilation than the medium dense samples. Figure 9a strongly indicates that during shearing the volume change response of the samples in both sands is dependent on the normal stress. The greater the loading, the lower the dilation. In addition, Table 2 shows that at similar initial relative densities, the SMol samples with higher void ratios are compressed easily, leading to having smaller dilation angles in comparison with the Mol samples. The maximum dilation angle (ψmax) ranges from 2.3° to 11.2° for the calcareous sand and 4.8° to 13.9° for the silica sand.

Interestingly, although the peak and residual strengths of the SMol samples are higher than those of the Mol samples, the Mol samples reach higher stresses than the SMol samples at small shear strains in the early state of shearing. This trend can be seen clearly in the dense samples (D_r = 80%). It is suggested that the various grain morphologies in the samples leading to greater particle interlocking and an increase in the number of inter-particle contacts causes the increase in shear strength properties for SMol sand, especially during the dilation process.

3.2.2 Effect of mean grain size D_{50} on the shear strength properties

The variation of the shear strength properties with the grain size for calcareous sand is shown in Figure 9b. In all the samples, the shear stress increases and reaches a residual state at γ = 10% without any indication of the peak. As expected, the vertical displacement is found to increase with increasing normal stress for all the samples. For each particle size, the results also show an increase in the residual friction angle at a higher normal stress, as summarized in Table 2. In Figure 9b, it is clear that the sample with larger particles having less SPH and stronger interlocking causes higher shear strength. In addition, the contractive and dilative behaviors of the samples are significantly dependent on normal stress. Although the shear stress reaches a residual state without any indication of the peak, the dilation occurs for the sample with larger particles under low normal stress. Under the normal stress of 50kPa, the sample with larger particles shows much more dilation phase than the sample with smaller particles, indicating that the dilation angle increases with increasing particle size under low load. However, this trend starts to divert under the higher normal stress of 100kPa, and finally, the completely opposite tendency is observed under 200kPa, where the sample of larger particles shows more contraction. This phenomenon is caused by the difference in particle movement, dependent on the particle size, and is explained as follows. Under a low normal stress, the sample with larger particles having greater particle hardness, greater particle angularity (or less particle SPH) and the uniformity of particle size in the sample can provide an interaction between the particles where the contact points of the particle edges (roughness) are strong enough to restrain the particle movement. However, under a higher load, the particle movement increases owing to the contributions of higher void ratio and particle polishing. In short, the volume change of the samples is dependent on the normal stress and the compression or dilation increases with the increase in particle size. Further, the relationship between shear strength properties and particle size is demonstrated in Figure 10a. It is observed that the shear strength and friction angle at residual state increase as the particle size increases for various normal stresses.

3.2.3 Correlations between shear strength properties and sphericity

Using Eq. 1, the SPHs interpolated for other uniform particle sizes are calculated and listed in Table 3.

Table 3. Particle characteristics of the tested sands.

Sand	Sieve size (mm)	D_{50} (mm)	Sphericity, SPH
S2	0.16-0.25	0.205	0.532
S3	0.315-0.5	0.408	0.517
S4	0.5-0.63	0.565	0.506
S5	0.63-1	0.815	0.485
S6	1-1.25	1.135	0.461

The correlations between the shear strength properties and particle shape corresponding to the effect of D_{50} are proposed for the calcareous sand under the various normal stresses (50, 100 and 200 kPa) shown in Figure 10b. The results show that the residual shear strength and friction angle decrease with an increasing SPH. Also, in Figure 10b the best-fit lines of the SPH and friction angle are proposed. The distance between the lines becomes smaller at higher normal stresses (100 and 200 kPa). It can be suggested that the correlations converge to a straight line under high normal stress.

4 CONCLUSIONS

The 3DA on the particles of the calcareous and silica sands is studied based on the data collected using X-ray CT. The particles of calcareous sand are found to show smaller sphericity (SPH) than those of silica and crushed calcareous sands. For calcareous sand, the particle shapes in descending order are blades, rods, discs and spheres; whereas silica sand contains more spheres and blades compared to rods and discs. These findings are consistent with the results obtained from the experiments of the maximum and minimum void ratios of the tested sands. It is proved that the SPH increases with decreasing grain size. However, in each sample, the smaller particles have lower SPH than the larger particles. Further, the 3DA gives smaller particle sizes than the sieve analysis (SA). Particle shape is found to be the main factor affecting the SA results. This is due to particle interlocking caused by various particle shapes, especially for the calcareous sand.

In this study, the correlations between the 3D particle shape and the size (D_{50}) are established. From the direct shear drained test results, the main conclusions can be drawn as follows:

- At the same C_u, the behavior of calcareous and silica sands are quite different. Although the calcareous sand with particles has more angularity and less SPH is formed at a higher void ratio, it gives higher peak and residual shear strength properties and tends to reach a lower shear strength at a small shear strain and a lower dilation than the silica sand. This tendency is seen clearly in the dense sample. The variety of particle shapes increases with the particle interlocking and the number of inter-particle contacts and causes increasing shear strength properties, especially during the dilation process.
- For calcareous sand, the increase in the particle size D_{50} leads to the growth in shear strength properties in the residual state. The compression and dilation curves of the calcareous sands are affected strongly by the normal stress. The range of compression and dilation phases increases with increasing particle size. The sample with larger particles, showing less particle movement for re-arrangement under low stress, causes more dilation, whereas the sample with smaller particles giving less particle movement under high stress shows less compression.
- The critical state may not be reached in this study. This supposes that the ultimate state for calcareous sand can be indicated at higher shear strain than silica sand.

REFERENCES

[1] Hassanlourad, M., Rasouli, M.R., Salehzadeh, H. 2014. A comparison between the undrained shear behavior of carbonate and quartz sands. Int. J. Civ. Eng. 12, 4, 338–350.

[2] Safinus, S., Hossain, M.S., Randolph, M.F. 2013. Comparison of stress-strain behaviour of carbonate and silicate sediments. Proc. 18th Int. Conf. on Soil Mechanics and Geotechnical Engineering, pp. 267–270.

[3] Brandes, H.G. 2011. Simple shear behavior of calcareous and quartz sands. Geotech. Geol. Eng. 29, 1, 113–126. DOI: 10.1007/s10706-010-9357-x

[4] Cho, G.C., Dodds, J., Santamarina, J.C. 2006. Particle shape effects on packing density, stiffness, and strength: natural and crushed sands. J. Geotech. Geoenvironmental Eng. 132, 5, 591–602. DOI: 10.1061/(ASCE)1090-0241(2006)132:5(591)

[5] Bui, M.T., Clayton, C.R.I., Priest, J.A. 2007. Effects of particle shape on Gmax of geomaterials. Proc. 4th Int. Conf. on Earthquake Geotechnical Engineering, No. 1536.

[6] Siang, A.J.L.M., Wijeyesekera, D.C., Zainorabidin, A., and Bakar, I. 2012. The effects of particle morphology (shape and sizes) characteristics on its engineering behaviour and sustainable engineering performance of sand. Int. J. Integr. Eng. 4, 3, 27–37.

[7] Miura, K., Maeda, K., Furukawa, M., Toki, S. (1998). Mechanical characteristics of sands with different primary properties. Soils Found. 38, 4, 159–172.

[8] Pettijohn, F.J., Lundahl, A.C. 1943. Shape and roundness of Lake Erie beach sands. J. Sediment. Res. 13, 2, 69–78. DOI: 10.1306/D426919D-2B26-11D7-8648000102C1865D

[9] Pollack, J.M. 1961. Significance of compo-

sitional and textural properties of South Canadian River channel sands, New Mexico, Texas, and Oklahoma. J. Sediment. Res. 31, 1, 15–37. DOI: 10.1306/74D70AEC-2B21-11D7-8648000102C1865D

[10] Das, N., Ashmawy, A.K. 2007. Relationship between grain size and shape of natural and crushed sand. Proc. of Geo-Denver 2007, New Peaks in Geotechnics, Denver, Colorado, United States, pp. 1–10. DOI: 10.1061/40917(236)25

[11] Barrett, P.J. 1980. The shape of rock particles: a critical review. Sedimentology 27, 3, 291–303. DOI: 10.1111/j.1365-3091.1980.tb01179.x

[12] Dewen, L., Yanrui, K., Dawei, L. 2015. Comparison of grain-size and grain-shape characters of alluvial and lakeshore sands based on dynamic image analysis. Quat. Sci. 35, 2, 484–492.

[13] Sun, Y., Indraratna, B., Nimbalkar, S. 2014. Three-dimensional characterization of particle size and shape for ballast. Geotech. Lett. 4, 197–202. DOI:10.1680/geolett.14.00036

[14] Yan, W.M., Dong, J. 2011. Effect of particle grading on the response of an idealized granular assemblage. Int. J. Geomech. 11, 4, 276–285. DOI: 10.1061/(ASCE)GM.1943-5622.0000085

[15] Lun, A.C.Y. 2011. Influence of grain size distribution on shear strength of sand. UG. Thesis, Universiti Teknologi Malaysia.

[16] Selig, E., Roner, C. 1987. Effects of particle characteristics on behavior of granular material. Transp. Res. Rec. 1131, 1–6.

[17] Madhavi Latha, G., Sitharam, T.G. 2008. Effect of particle size and gradation on the behaviour of granular materials simulated using DEM. Indian Geotech. J. 38, 1, 68–88.

[18] Ueda, T., Matsushima, T., Yamada, Y. 2011. Effect of particle size ratio and volume fraction on shear strength of binary granular mixture. Granul. Matter. 13, 6, 731–742. DOI: 10.1007/s10035-011-0292-1

[19] Pakbaz, M.S., Moqaddam, A.S. 2012. Effect of sand gradation on the behavior of sand-clay mixtures. Int. J. GEOMATE 3, 1, 325–331.

[20] Alias, R., Kasa, A., Taha, M.R. 2014. Particle size effect on shear strength of granular materials in direct shear test. Int. J. Civil. Env. Struct. Constr. Archit. Eng. 8, 11, 733–736.

[21] Li, Y., Huang, R., Chan, L.S., Chen, J. 2013. Effects of particle shape on shear strength of clay-gravel mixture. KSCE J. Civ. Eng. 17, 4, 712–717. DOI: 10.1007/s12205-013-0003-z

[22] Kara, E.M. 2013. Contribution of particles size ranges to sand friction. Eng. Technol. Appl. Sci. Res. 3, 4, 497–501.

[23] Vangla, P., Madhavi, G. 2015. Influence of particle size on the friction and interfacial shear strength of sands of similar morphology. Int. J. Geosynth. Gr. Eng 1, 1, 1–12. DOI: 10.1007/s40891-014-0008-9

[24] Desrosiers, R., Silva, A.J. 2002. Strength behavior of marine sands at elevated confining stresses. Mar. Georesources Geotechnol. 20, 1, 1–19. DOI: 10.1080/106411902753556834

[25] Ghionna, V.N., Caridi, G., Porcino, D. 2008. Undrained monotonic and cyclic simple shear behaviour of carbonate sand. Géotechnique 58, 8, 635–644. DOI: 10.1680/geot.2007.00036

[26] Cabalar, A.F., Dulundu, K., Tuncay, K. 2013. Strength of various sands in triaxial and cyclic direct shear tests. Eng. Geol. 156, 92–102. DOI: 10.1016/j.enggeo.2013.01.011

[27] Potticary, M., Zervos, A., Harkness, J. 2016. The Effect of particle elongation on the strength of granular materials. Proc. 24th UK Conf. Association for Computational Mechanics in Engineering, pp. 31–34.

[28] ASTM D 4253-00. 2006. Standard test methods for maximum index density and unit weight of soils using a vibratory table. ASTM International, West Conshohocken, PA, USA.

[29] Masschaele, B.C., Cnudde, V., Dierick, M., Jacobs, P., Van Hoorebeke, L., Vlassenbroeck, J. 2007. UGCT: New X-ray radiography and tomography facility. Nucl. Instruments Methods Phys. Res., Section A: Accelerators, Spectrometers, Detectors and Associated Equipment 580, 1, 266–269. DOI: 10.1016/j.nima.2007.05.099

[30] Vlassenbroeck, J., Dierick, M., Masschaele, B., Cnudde, V., Van Hoorebeke, L., Jacobs, P. 2007. Software tools for quantification of X-ray microtomography at the UGCT. Nucl. Instruments Methods Phys. Res., Section A: Accelerators, Spectrometers, Detectors and Associated Equipment 580, 1, 442–445. DOI: 10.1016/j.nima.2007.05.073

[31] Cnudde, V., Dewanckele, J., De Boever, W., Brabant, L., De Kock, T. 2012. 3D characterization of grain size distributions in sandstone by means of X-ray computed tomography. Quant. Mineral. Microanal. Sediments Sediment. Rocks 42, 99–113.

[32] Illenberger, W.K. 1991. Pebble shape (and size!). J. Sediment. Res. 61, 5, 756–767. DOI: 10.1306/D42677C6-2B26-11D7-8648000102C1865D

[33] Brabant, L., Vlassenbroeck, J., De Witte, Y., Cnudde, V., Boone, M., Dewanckele, J., Van Hoorebeke, L. 2011. Three-dimensional analysis of high-resolution X-ray computed tomography data

with Morpho+. Microscopy and Microanalysis 17, 2, 252–63. DOI: 10.1017/S1431927610094389

[34] JIS A 1224. 2009. Test method for minimum and maximum densities of sands. Japanese Geotechnical Society, Soil Testing Standards, Tokyo, pp.136-138.